Title:
Theoretical modelling of Raman spectra

Running title:
Theoretical Raman

Table of contents:

1. Introduction....2
2. Lattice dynamics and phonons....3
3. Phonon calculations using ab initio methods....7
   3.1. Density functional theory....7
   3.2. Density functional perturbation theory....8
   3.3. Perturbation expansion....8
   3.4. From mixed perturbations to physical properties....10
4. Raman tensors and Raman spectra....11
5. Examples....13
6. The WURM project....14
Acknowledgements....15
References....15

Corresponding author:

Razvan CARACAS,
Centre National de la Recherche Scientifique, Ecole Normale Supérieure de Lyon, Laboratoire de Géologie, UMR 5276, 46 allée d'Italie, 69364, Lyon cedex 07, France
e-mail: razvan.caracas@ens-lyon.fr,

File format:

Word document "RamanCaracas.doc", Mac OS

Theoretical modelling of Raman spectra

Razvan Caracas and Ema Bobocioiu

Ecole Normale Supérieure de Lyon, Laboratoire de Géologie de Lyon, CNRS UMR 5276, 46 allee d'Italie, 69364, Lyon cedex 07, France

The atomic lattices are not static ensemble of atoms, but rather the atomic nuclei in solids are always vibrating. Various factors like temperature, external electric or magnetic fields, pressure, *etc*. can affect these vibrations. The pattern of vibrations is structural- and compound-dependent. Consequently one of its possible uses is determinative, as recorded in Raman and/or infrared spectra. Here we briefly present the theoretical basis of lattice dynamics in the density-functional perturbation theory formalism. Then we discuss in detail the formalism used to compute the Raman spectra, with both peak position and intensity. We exemplify with the WURM project, a web-based freely available repository of computed physical properties for minerals, focused around the Raman spectra.

1. Introduction

Mineral structures, just like any other solid crystalline lattices, are periodic collections of atoms, whose state is in continuous movement around some average equilibrium positions. The time average of these movements, of these fluctuations, is related to the thermal agitation tensors, as measured for example in various diffraction techniques. This average can also be decomposed in a collection of well-defined normal modes of vibration (Rull et al., 2012). The amplitudes and the patterns of atomic displacements are ruled by the inter-atomic interactions and the lattice symmetry. This makes them a very powerful tool in mineral identification. Vibrational spectroscopies, like Raman and infrared, are employed to sample specific subsets of the vibrational pattern. Provided reference spectra are available, they can be successfully used for identification purposes.

Moreover, when integrated the full vibrational pattern yields standard thermodynamic parameters, like specific heat, free energy *etc*. (Maradudin *et al*., 1971). Various external factors, like strains, temperature, electric and magnetic fields, *etc*. can affect the vibrational state of the lattice, inducing changes that lead all the way up to phase transitions. In this way one is able to build the full phase diagram and to characterize the entire dynamical properties of a solid provided information about the vibrational spectrum is known.

The vibrational spectrum can be measured by various vibrational spectroscopies or can be calculated by treating the fluctuations described above as perturbations of a static well-defined lattice. The static lattice can be fully characterized using ab initio techniques based on the density functional theory (Hohenberg & Kohn, 1964; Kohn & Sham, 1965). The fluctuations can then be described inside the density functional-perturbation theory (Baroni *et al*., 1987; Gonze & Vigneron, 1989; Gonze *et al*., 1992; de Gironcoli, 1995; Gonze, 1995, 1997; Gonze & Lee, 1997; Putrino *et al*., 2000; Baroni *et al*., 2001; Gonze *et al*., 2005).

In the following pages we focus on the computation of the Raman and infrared spectra using density-functional perturbation theory. We briefly review the theory of phonons (Section 2). We then discuss the basics of the density-functional theory (Section 3.1), on which we build the foundations of the density-functional perturbation theory (Section 3.2). We describe the perturbation expansion of the density-functional theory in Section 3.3 and show the relation between its various terms and the physical properties of a lattice in Section 3.4. The relation between the computed Raman tensors and the Raman spectra is discussed in Section 4. We end with an overview of the WURM project in Section 5, which proposes a database of computed Raman spectra and other derived physical properties for minerals.

2. Lattice dynamics and phonons

The static lattice at equilibrium is characterized by minimum enthalpy at a given pressure, i.e. density, and by zero forces acting on the atoms. Any perturbation of this state induces the development of interatomic forces and, if that given structure is the stable structure at that pressure, by an increase in energy. The atomic vibrations can be described as small perturbations around the positions of equilibrium (Maradudin, 1971; Baroni *et al*., 1987; Srivastava, 1990; Gonze & Lee, 1997; Baroni *et al*., 2001; Gonze *et al*., 2005). Studying the changes in energy associated to these perturbations yields the amplitude and displacement pattern of the vibrations.

Figure 1 shows the three possible behaviours. We represent on the horizontal axis the displacement (λ) of one particular atom away from its position of equilibrium (at $\lambda = 0$). The vertical axis shows the variation of the energy. The force F along direction α acting on the atom a from the cell κ can be described as the first derivative of the energy E with respect to the displacement of that atoms from its equilibrium position τ_κ:

$$F^a_{\kappa\alpha} = \frac{\partial E}{\partial \tau^a_{\kappa\alpha}} \qquad (1)$$

In case of a stable structure, as the atoms are taken away from their equilibrium positions, the energy of the structure increases. Consequently, forces develop that tend to push back the atoms in their original positions. The structure is then stable and the atoms vibrate around these positions of equilibrium, subject to symmetry. This case is represented by the continuous curve in Figure 1, depicting a single-well potential. The bottom of the well corresponds to the atomic equilibrium position. The curvature of the potential line, i.e. the second order derivative of the energy with respect to atomic displacements, is related to the square of the frequency of the vibration. The frequency is then a positive number; the structure is dynamically stable. For the same atomic mass, narrower is the potential higher is the vibrational frequency. The full description of the vibrational pattern yields the thermodynamical parameters, as explained further below. This implies that a dynamically stable structure is thermodynamically metastable if it does not have the lowest Gibbs free energy.

If a structural instability starts to develop, a soft phonon mode may occur. In terms of energy behaviour this can be seen as the opening of the continuous curve. In

this case (the dotted curve in Figure 1), the forces acting on atoms that tend to drag them back into their equilibrium positions would be very small, zero in the limit case of a flat curve. That means that any distortion seen as a perturbation of the structure would be preserved as such and the initial equilibrium positions are lost. This corresponds to the appearance of a soft mode in a structure, precursor to a second-order phase transition (Landau & Lifschits, 1960; Srivastava, 1990).

Eventually this flattening can fully transform into a double-well potential, as shown by the dashed curve of the Figure 1. In this extreme case a displacement of the atom from its initial position results in a force that will drag it away from the starting point. The atom will then follow the path of lowest energy to find a new position of minimum energy, thus a new position of equilibrium. This corresponds to a phase transition, namely a second order phase transition. The frequency of the corresponding vibrational mode is imaginary, as its square is negative. It is a soft mode.

Based on this reasoning we can then express the energy of a lattice as a Taylor-series expansion as a function of small atomic displacements around the equilibrium positions. If the series is truncated at the third fourth order we obtain the following expression for the energy:

$$E = E^{(0)} + \sum_{a\kappa\alpha}\left(\frac{\partial E}{\partial \tau^{a}_{\kappa\alpha}}\right)\Delta\tau^{a}_{\kappa\alpha} + \sum_{a\kappa\alpha}\sum_{b\kappa'\beta}\left(\frac{\partial^2 E}{\partial \tau^{a}_{\kappa\alpha}\partial \tau^{b}_{\kappa'\beta}}\right)\Delta\tau^{a}_{\kappa\alpha}\Delta\tau^{b}_{\kappa'\beta} +$$
$$\sum_{a\kappa\alpha}\sum_{b\kappa\beta}\sum_{c\kappa''\gamma}\left(\frac{\partial^3 E}{\partial \tau^{a}_{\kappa\alpha}\partial \tau^{b}_{\kappa'\beta}\partial \tau^{c}_{\kappa''\gamma}}\right)\Delta\tau^{a}_{\kappa\alpha}\Delta\tau^{b}_{\kappa'\beta}\Delta\tau^{c}_{\kappa''\gamma} + \qquad (2)$$
$$\sum_{a\kappa\alpha}\sum_{b\kappa'\beta}\sum_{c\kappa''\gamma}\sum_{dk'''\gamma}\left(\frac{\partial^4 E}{\partial \tau^{a}_{\kappa\alpha}\partial \tau^{b}_{\kappa'\beta}\partial \tau^{c}_{\kappa''\gamma}\partial \tau^{d}_{\kappa''''\lambda}}\right)\Delta\tau^{a}_{\kappa\alpha}\Delta\tau^{b}_{\kappa'\beta}\Delta\tau^{c}_{\kappa''\gamma}\Delta\tau^{d}_{\kappa''''\lambda}$$

In this expression the first term, $E^{(0)}$, corresponds to the static energy of the unperturbed lattice. The second term is the first derivative of the energy that yields the forces acting on the atoms. This term is zero for a structure at equilibrium. The third term is the second derivative of the energy with respect to two atomic displacements; this yields the curvature of the three coloured lines in Figure 1. It is of central interest in our following discussion for determining the phonon frequencies and corresponding atomic displacement patterns. This third term is also called *harmonic* because of the parallel with an elastic resort detailed below. The truncation of the Taylor series immediately after the harmonic term is called the *harmonic approximation*. It describes the lattice as quasi-elastic where the interatomic forces and the phonons are not damped. In this case the interactions between the atoms are elastic (Figure 2).

The fourth and fifth terms are the first anharmonic term. If calculated they give the phonon lifetimes and Raman/infrared peak widths. In particular the fourth-order derivatives are involved in the computation of the phonon-phonon interactions and of the lattice heat conductivity. Further higher terms in the series expansion give various better corrections for anharmonicities.

In the harmonic approximation then we can write the following relations to obtain the phonon frequencies. The force on the atom κ, that arises because of the displacement of another atom κ' (which can also be itself) can be expressed as:

$$F^a_{\kappa\alpha} = -\sum_{b\kappa'\beta}\left(\frac{\partial^2 E}{\partial\tau^a_{\kappa\alpha}\partial\tau^b_{\kappa'\beta}}\right)\Delta\tau^b_{\kappa'\beta} \tag{3}$$

There is an one-to-one parallel to the case of an elastic lattice, where the elastic force ($F = -kx$, with k the elastic constant and x the displacement around the equilibrium position) can be expressed as:

$$F^a_{\kappa\alpha} = -\sum_{b\kappa'\beta} C_{\kappa\alpha,\kappa'\beta}(a,b)\Delta\tau^b_{\kappa'\beta} \tag{4}$$

where the matrix $\boldsymbol{C}$ represents the matrix of interatomic force constants (IFC), containing the elastic-like constants of all interatomic interactions as represented in Figure 2:

$$C_{\kappa\alpha,\kappa'\beta}(a,b) = \left(\frac{\partial^2 E}{\partial\tau^a_{\kappa\alpha}\partial\tau^b_{\kappa'\beta}}\right) \tag{5}$$

With the atoms under the influence of forces, the classical Newtonian formalism F = mass times acceleration can be applied in this case:

$$F^a_{\kappa\alpha}(t) = M_\kappa \frac{\partial^2\tau^a_{\kappa\alpha}(t)}{\partial t^2} \tag{6}$$

where M_κ is the mass of atom κ.

Then the two expressions of the forces, elastic and Newtonian can be equated as:

$$-\sum_{b\kappa'\beta}\left(\frac{\partial^2 E}{\partial\tau^a_{\kappa\alpha}\partial\tau^b_{\kappa'\beta}}\right)\Delta\tau^b_{\kappa'\beta} = M_\kappa \frac{\partial^2\tau^a_{\kappa\alpha}(t)}{\partial t^2} \tag{7}$$

This forms a system of differential equations:

$$\sum_{\kappa'\beta b} C_{\kappa\alpha,\kappa'\beta}(a,b)U^b_\sigma(\kappa'\beta) = M_\kappa\omega^2_\sigma U^a_\sigma(\kappa\alpha) \tag{8}$$

The solution of this system of equations represents a set of period elastic waves that correspond to atomic vibrations around their positions of equilibrium with some specific frequencies. They form the normal modes of vibration and are described as:

$$\Delta\tau^a_{\kappa\alpha}(t) = \sum_\sigma A_\sigma U^a_\sigma(\kappa\alpha)e^{i\omega_\sigma t} + ct \tag{9}$$

where σ labels the normal modes, A_σ their amplitude, ω_σ their normal mode angular frequency, and ct is a constant. The pattern of the atomic displacements is set by $U^a_\sigma(\kappa\alpha)$. Due to translational invariance of the crystalline lattice, the interatomic force constant between the atoms κ and κ' respectively from cells a and b is equal to that between atoms κ and κ' respectively from cell a' and b', if the two pair of cells a,

b and *a*', *b*' are separated by the same lattice vector, denoted by *q*. Then the *a*-*b* and the *a*'-*b*' difference can be replaced by **q**, which is the wavevector of the normal modes of vibration. These normal modes are the product of a wavevector-dependent phase factor that varies from cell to cell, with a wavevector-dependent periodic function. Consequently they have the form of Bloch waves and are quantized:

$$U_{\sigma}^{a}(\kappa\alpha) = e^{i\mathrm{q}.\mathrm{R}_a} U_{m\mathrm{q}}(\kappa\alpha) \tag{10}$$

These displacements represent the phonons. In practice they are obtained from the diagonalization of a set of equations:

$$\sum_{\kappa'\beta} D_{\kappa\alpha,\kappa'\beta}(\mathrm{q}) U_{m\mathrm{q}}(\kappa'\beta) = M_{\kappa}\omega_{m\mathrm{q}}^{2} U_{m\mathrm{q}}(\kappa\alpha) \tag{11}$$

that involve the dynamical matrices, which are the Fourier transforms of the interatomic force constants matrices at particular $a - b = q$ vectors:

$$D_{\kappa\alpha,\kappa'\beta}(\mathrm{q}) = \sum_{b} C_{\kappa\alpha,\kappa'\beta}(0,b) e^{i\mathrm{q}.\mathrm{R}_b} \tag{12}$$

The dynamical matrix is square with dimension $3N \times 3N$, where N is the number of nuclei in the unit cell and 3 comes form the three directions of the space. Its diagonalization yields the eigenvalues, which are the square of the phonon frequencies, and the eigenvectors, which are the atomic displacements corresponding to the vibrations. Each eigenvector has $3N$ components, corresponding to the displacement of each of the N atoms along the three Cartesian directions. The phonons, also named phonon modes, can be degenerated, symmetry allowed. The full symmetry description of the phonons modes can be done using the irreducible representations (e.g. Pawley, 1974; Perez-Mato *et al*., 1998; Kroumova *et al*., 2003, Rull et al., 2012). It is particularly useful to describe the phonon modes for $q = 0$, as they are sampled using Raman and infrared spectroscopies.

The representation of the phonon frequencies as a function of wavevector q corresponds to the dispersion relations that form the phonon band structures. As for all waves propagating in a periodic medium, e.g. electronic wave, the wavevectors are restricted to the Brillouin zone, the smallest periodic cell of the reciprocal lattice delimited by Bragg planes. As for electrons, the phonon dispersion relations are represented for a selected set of high symmetry lines in the Brillouin zone.

From all the points of the Brillouin zone, the centre, $q = \langle 000 \rangle$ labelled the Γ point is of particular interest. The phonons with wavevector Γ have identical displacement patterns in all unit cells of the lattice. By contrast, all the other points in the Brillouin zone correspond to waves with a finite wavelength and a phase varying from cell to cell, i.e. propagating waves. There are three phonon branches, called acoustic, that go to zero frequency when q approaches 0. For these modes all atoms have identical displacements along each of three Cartesian directions. Due to the translational invariance the structure is left invariant and the frequency of these modes is zero. The dispersion of these modes (measured for example in Brillouin spectroscopy) is related to the elastic constants tensor and eventually to the velocity of the acoustic waves travelling through the crystal.

Before going any further let us spend a little more time on the truncation of the Taylor series and on its effects on the phonon description. In the harmonic approximation, because of the missing third and higher order derivatives, the potential wells are symmetrical around the atomic equilibrium positions, as shown in Figure 1.

However in reality these wells are asymmetric, because the repulsion and attraction components of the interatomic interactions are not symmetrical. Figure 3 shows the asymmetric real potential well and the symmetric potential wells around the H atom in the real case of brucite, $Mg(OH)_2$ (Reynard & Caracas, 2009, Reynard, 2012). The effect of asymmetrization changes the curvature at zero and thus eventually affects the phonon frequency – one of the main reasons the computed phonon frequencies disagree with the measured ones. The difference between the two curves is one of the major causes for discrepancies between the computed and the measured phonon frequencies. Considering high-order terms in the Taylor expansion increases the agreement between the two techniques. But for most of the physical applications and crystal structures the quasiharmonic approximation gives already meaningful results.

3. Phonon calculations using ab initio methods

The computation of the energy of a static lattice and of the dynamical matrix at one specific q wavevector are now routine tasks, if performed in the framework of respectively the density functional theory (DFT) and the density functional perturbation theory (DFPT). As dealing with general q wavevectors goes beyond the purpose of the present chapter (see further in Gonze *et al*., 2005; Caracas & Gonze, 2010), in this chapter, we will concentrate only on the determination of the phonons in Γ in the framework of the DFT and the DFPT.

3.1. Density functional theory

The basis of DFT have been put in the mid-sixties, when Hohenberg & Kohn (1964) and Kohn & Sham (1965) established an energy formulation that is in one-to-one correspondence with the Schrödinger equation, but is a functional of the density and not of the many-body electronic wavefunction. The Kohn-Sham, or DFT, equation gives the ground-state energy of a static lattice as (Kohn & Sham, 1964; Payne *et al*., 1992; Martin, 2004):

$$E[n(r)] = T_s[n(r)] + E_{ext}[n(r)] + E_{col}[n(r)] + E_{xc}[n(r)] \tag{13}$$

where the terms on the right side represent in order the kinetic energy, the interaction with the external fields, the Coulombian energy and the exchange-correlation energy. The Coulombian energy contains the interactions between the electrons, between the nuclei and between the electrons and nuclei. The many-body aspects of the Schrödinger equation are in the exchange-correlation energy, whose expression is not analytical. Rather approximation, *e.g*. the local density approximation and the generalized gradient approximation, are used to estimate the value of this term. The electron density $n(r)$ is given as a function of the groundstate wavefunctions $\psi(r,r_2,r_3,...,r_N)$ as:

$$n(r) = \int d^3r_2 \int d^3r_3 ... \int d^3r_N \psi^*(r,r_2,r_3,....,r_N)\psi(r,r_2,r_3,...,r_N) \tag{14}$$

In practice, one finds the electron density distribution that minimizes the Kohn-Sham equation for one lattice.

3.2. Density functional perturbation theory

In the DFPT the derivatives of the DFT electronic energy are computed with respect to different perturbations. The nuclei-nuclei interaction energy is then added by computing the electrostatic repulsion between classical point charges.

The perturbations treated in DFPT might be changes of potentials induced by nuclear displacements, or external applied electric and magnetic fields, strains, as well as any type of perturbation of the equations that define the reference system. This powerful generic theory is able to deal with perturbations characterized by any wavevector, zero or non-zero, commensurate or even incommensurate (Caracas & Gonze, 2005). The computing effort is independent of the perturbation wavevector, and consequently, this method is very efficient for dealing with phonons.

3.3. Perturbation expansion

The DFT equations have been defined for generic external potentials v_{ext}. We now choose a reference (unperturbed) external potential v_{ext} and expand the perturbed potential v_{ext} in terms of a small parameter λ, as follows (Gonze & Vigneron, 1989; Gonze, 1995):

$$v_{ext}(\lambda) = v_{ext}^{(0)} + \lambda v_{ext}^{(1)} + \lambda^2 v_{ext}^{(2)} + \lambda^3 v_{ext}^{(3)} + \lambda^4 v_{ext}^{(4)} + ... \quad (15)$$

The perturbation can be for example atomic displacements, external electric fields, deformations, etc. We are interested in the changes of physical quantities ($X(\lambda)$), due to the perturbation of the external potential (Altman, 1991). They are similarly expanded as:

$$X(\lambda) = X^{(0)} + \lambda X^{(1)} + \lambda^2 X^{(2)} + \lambda^3 X^{(3)} + \lambda^4 X^{(4)} + ... \quad (16)$$

where X can be the electronic energy, the electronic wavefunctions, the density, the electron eigenenergies or the Hamiltonian. The first term, zeroth-order, of the series is then (α label the electronic states):

$$H^{(0)} \mid \psi_\alpha^{(0)} >= \varepsilon_\alpha^{(0)} \mid \psi_\alpha^{(0)} > \quad (17)$$

or equivalently:

$$< \psi_\alpha^{(0)} \mid H^{(0)} \mid \psi_\alpha^{(0)} >= \varepsilon_\alpha^{(0)} \quad (18)$$

By derivation, we obtain:

$$<\psi_\alpha^{(1)}|H^{(0)}|\psi_\alpha^{(0)}>+<\psi_\alpha^{(0)}|H^{(1)}|\psi_\alpha^{(0)}>+<\psi_\alpha^{(0)}|H^{(0)}|\psi_\alpha^{(1)}>=\varepsilon_\alpha^{(1)} \quad (19)$$

Because $<\psi_\alpha^{(0)}|\psi_\alpha^{(0)}>=1$, its derivative is null:

$$<\psi_\alpha|\psi_\alpha>^{(1)}=<\psi_\alpha^{(1)}|\psi_\alpha^{(0)}>+<\psi_\alpha^{(0)}|\psi_\alpha^{(1)}>=0 \quad (20)$$

On this basis (Equation 20), the first and the third terms of the left side of Equation 19 vanish. The first-order term for energy becomes:

$$E^{(1)}=\sum_\alpha^{occ}<\psi_\alpha^{(0)}|H^{(1)}|\psi_\alpha^{(0)}> \quad (21)$$

Because of the nature of the external perturbation this is equivalent to:

$$E_{el}^{(1)}=\sum_\alpha^{occ}<\psi_\alpha^{(0)}|v_{ext}^{(1)}|\psi_\alpha^{(0)}> \quad (22)$$

and its corresponding electronic wavefunctions and density are determined self-consistently, step by step. All the terms in the Taylor development of the energy can be determined using this procedure.

Moreover, the existence of one perturbation induces a coupling of other perturbation as well. For example, during the atomic vibrations, there is a coupling between phonons and (induced) electric field. Then mixed derivatives of the energy with respect to both atomic displacements and homogeneous electric fields are required for computation of vibrations.

Equation 15 is re-written to take into account such mixed derivatives. The Taylor expansion of the perturbations can be combined as:

$$v_{ext}(\lambda)=v_{ext}^{(0)}+\sum_{j_1}\lambda_{j_1}v_{ext,j_1}+\sum_{j_1,j_2}\lambda_{j_1}\lambda_{j2}v_{ext,j_1j_2}+\sum_{j_1,j_2j_3}\lambda_{j_1}\lambda_{j2}\lambda_{j3}v_{ext,j_1j_2j_3}+\sum_{j_1j_2j_3j_4}\lambda_{j_1}\lambda_{j2}\lambda_{j3}\lambda_{j4}v_{ext,j_1j_2j_3j_4}+\ldots \quad (23)$$

The mixed derivatives of the energy of the electronic system have the form:

$$E_{el,j_1j_2}=\frac{1}{2}\frac{\partial^2 E_{el}}{\partial\lambda_{j_1}\partial\lambda_{j_2}} \quad (24)$$

and are obtained from:

$$E^{j_1j_2}=\sum_\alpha<\psi_\alpha^{j_2}|v_{ext}^{j_1}|\psi_\alpha^{(0)}>+\sum_\alpha<\psi_\alpha^{(0)}|v_{ext}^{j_1j_2}|\psi_\alpha^{(0)}> \quad (25)$$

In equation 26, the first-order derivatives of the wavefunctions with respect to the first perturbation are not needed. When three perturbations are considered (*e.g.* two electric fields and one atomic displacement in case of Raman tensors or three electric field in case of non-linear optical coefficients) the latter expression becomes:

$$E_{el}^{j_1j_2j_3}=\frac{1}{3}\frac{\partial^3 E_{el}}{\partial\lambda_{j_1}\partial\lambda_{j_2}\partial\lambda_{j_3}} \quad (26)$$

Thus, the ability to compute the first-order responses (i.e., changes in wavefunctions and densities) to the basic perturbations gives us also, as by-products, mixed higher order derivatives of the electronic energy (Gonze & Vigneron, 1989; Baroni *et al*., 2001).

3.4. From mixed perturbations to physical properties

Raman spectroscopy is the measurement of the scattering of an incoming electromagnetic radiation, namely a laser, by the normal modes of vibration. Consequently, computing the Raman effect needs to take into account the presence of an external electric field that acts as a second perturbation to the system (the first is the nuclear vibrations). The presence of this external field changes the enthalpy of the system. Explicitly, it is necessary to define a variational electronic enthalpy that contains both the electronic energy (from DFT) and its changes under this external electric field (Nunes & Gonze, 2001):

$$F_{e+i}[\mathbf{R}_k,\boldsymbol{\mathcal{E}}] = \min_{\psi_n}(E_{e+i}[\mathbf{R}_k,\psi_k] - \Omega_0 \boldsymbol{\mathcal{E}} P[\psi_k] \tag{27}$$

where Ω_0 is the unit cell volumes, $\boldsymbol{\mathcal{E}}$ is the external electric field and $P[\psi_k]$ is the induced polarization. In this framework, the energy of the crystal is replaced by this new expression of the electronic enthalpy and Equation 2, expressed as a Taylor expansion to third order, becomes:

$$F_{e+i}[\lambda] = F_{e+i}^{(0)}[\lambda] + \sum_i \left(\frac{\partial F_{e+i}}{\partial \lambda_i}\right)\lambda_i + \frac{1}{2}\sum_{ij}\left(\frac{\partial^2 F_{e+i}}{\partial \lambda_i \partial \lambda_j}\right)\lambda_i\lambda_j + \frac{1}{6}\sum_{ij}\left(\frac{\partial^3 F_{e+i}}{\partial \lambda_i \partial \lambda_j \partial \lambda_k}\right)\lambda_i\lambda_j\lambda_k \tag{28}$$

With the perturbations being the atomic displacements $\boldsymbol{\tau}$ and the electric fields, each of the different terms of the full expansion corresponds to a measurable physical property, as follows:

$$\begin{aligned}
&F_{e+i}[\mathrm{R}_k,E] = F_{e+i}^{(0)}[\mathrm{R}_k,E] \\
&-\Omega_0 \sum_{\alpha} \underbrace{P_\alpha^s}_{polarization}\ \mathcal{E}_\alpha - \sum_\alpha \sum_k \underbrace{F_\alpha^0 \tau_{\kappa\alpha}}_{forces} \\
&-\Omega_0/2 \sum_{\alpha\beta} \underbrace{\chi_{\alpha\beta}^{\infty(1)}}_{dielectric\ tensor} \mathcal{E}_\alpha \mathcal{E}_\beta - \sum_{\alpha\beta}\sum_\kappa \underbrace{Z^*_{\kappa,\alpha\beta}}_{dynamical\ \mathrm{charges}} \tau_{\kappa\alpha}\mathcal{E}_\beta + 1/2 \sum_{\alpha\beta}\sum_{\kappa'\kappa} \underbrace{C_{\alpha\beta}(\kappa,\kappa'')}_{\mathrm{int}\ eratomic\ force\ cts.} \tau_{\kappa\alpha}\tau_{\kappa'\beta} \\
&-\Omega_0/3 \sum_{\alpha\beta} \underbrace{\chi_{\alpha\beta\gamma}^{\infty(2)}}_{Non-linear\ opt.\ coeff.} \mathcal{E}_\alpha \mathcal{E}_\beta \mathcal{E}_\gamma - \Omega_0/2 \sum_\kappa \sum_{\alpha\beta} \underbrace{\frac{\partial \chi_{\alpha\beta}^{\infty(1)}}{\partial \tau_{\kappa\gamma}}}_{Raman\ coeff.} \mathcal{E}_\alpha \mathcal{E}_\beta \tau_{\kappa\gamma} \\
&-1/2 \sum_{\kappa\kappa'}\sum_{\alpha\beta} \frac{\partial Z^*_{\kappa,\alpha\beta}}{\partial \tau_{\kappa'\gamma}} \tau_{\kappa\alpha}\tau_{\kappa'\beta}\mathcal{E}_\beta + 1/3 \sum_{\kappa\kappa'\kappa''}\sum_{\alpha\beta} \underbrace{\Xi(\kappa,\kappa',\kappa'')}_{anharmonicities} \tau_{\kappa\alpha}\tau_{\kappa'\beta}\tau_{\kappa''\gamma} + \ldots.
\end{aligned} \tag{29}$$

Inverting this equation yields the different physical properties of interest.

The terms of the Taylor expansion up to the second order are computed using DFTP briefly outlined above. The third order terms can be computed within the same approach, using the 2n+1 theorem (Gonze & Vigneron, 1989). The complexity of evaluating each higher-order term of the Kohn-Sham equations and consequently the complexity of the implementation increase with the order of the derivation. Currently, there are several available implementations of the non-linear optical coefficients, *i.e.* the derivative of the energy with respect to three electric fields, and of the Raman tensors, *i.e.* the derivative of the energy with respect to two electric fields and one with respect to atomic displacements (Baroni & Resta, 1986; Lazzeri & Mauri 2003; Veithen *et al.*, 2005). The third term of the third order derivative of the energy, *i.e.* with respect to one electric field and two atomic displacements, participates to the width of the infrared and Raman peaks, while the very last term from the expression yields anharmonicities, related to the phonon life time, the line broadening of Raman and infrared spectra and thermal transport due to phonon scattering. However the exact calculation of these latter properties needs the knowledge of the fourth order derivatives, too.

4. Raman tensors and Raman spectra

The Raman intensity of a specific mode m is determined by the specific Raman scattering efficiency (S) via a prefactor. The Raman scattering efficiency depends on the frequency of the incoming photon, ω_0, on the frequency of the phonon, ω_m, on temperature, T, and on the Raman tensor α^m of that particular mode m. Its full expression is (Cardona, 1982; Placzek, 1934; Hayes & Loudon, 1978):

$$\frac{dS_m}{dV} = \frac{(\omega_0 - \omega_m)^4}{c^4} |\mathrm{e_S} \cdot \alpha^m \cdot \mathrm{e_0}|^2 \frac{h}{2\omega_m}(n_m + 1) \tag{30}$$

e_s and e_0 are the orientations of the respectively scattered and incident light, i.*e*. laser. The dependency on temperature is given by the boson factor:

$$n_m = \frac{1}{e^{h\omega_m / k_B T} - 1} \tag{31}$$

and the Raman tensor:

$$\alpha_{ij}^m = \sqrt{\Omega_0} \sum_{\kappa\beta} \frac{\partial \chi_{ij}^{\infty(1)}}{\partial \tau_{\kappa\beta}} \eta_m(\kappa\beta) = \sqrt{\Omega_0} \sum_{\kappa\beta} \frac{\partial}{\partial \tau_{\kappa\beta}} \left(\frac{\partial^2 E}{\partial \mathcal{E}_i \partial \mathcal{E}_j} \right) \mathcal{E}_i \mathcal{E}_j \eta_m(\kappa\beta) \tag{32}$$

is the derivative of the macroscopic dielectric tensor with respect to the set of atomic displacements that correspond to the phonon eigenvector (Baroni & Resta, 1986; Lazzeri & Mauri, 2003; Veithen *et al.*, 2005). The middle term in Eq. (27),

$|e_S \cdot \alpha^m \cdot e_0|$, gives the coupling between the incoming phonon with polarization e_0, the crystal, characterized by a Raman tensor α^m of phonon mode *m* and the scattered phonon with polarization e_s.

The Raman tensors are the key ingredients needed to calculate the Raman spectra. They can be computed either from finite differences, as the change of the dielectric tensor due to infinitesimal atomic displacements, or from perturbation theory, as the derivative of the energy with respect to three perturbations: two electric fields and one atomic displacement.

Concerning the Raman spectra, the Raman tensor is given by the Raman coefficient term. For non-centrosymmetric crystals, some modes are active in both Raman and infrared. In this case, the same formalism as above holds for the transverse optical (TO) component (i.e. a phonon mode that yields a dipole moment oriented perpendicular to the direction of the incoming laser), while a supplementary correction is needed for the modes in longitudinal optical (LO) geometry (i.e. a phonon mode that yields a dipole moment oriented parallel to the direction of the incoming laser). In this case the Raman tensors become (Veithen *et al*., 2005):

$$\left.\frac{\partial \chi_{ij}^{\infty(1)}}{\partial \tau_{\kappa\beta}}\right|_{D=0} = \left.\frac{\partial \chi_{ij}^{\infty(1)}}{\partial \tau_{\kappa\beta}}\right|_{E=0} - \frac{8\pi}{\Omega_0} \frac{\sum_l Z^*_{\kappa\beta l} q_l}{\sum_{ll'} q_l \varepsilon^{\infty}_{llj'} q_{l'}} \sum_l \chi^{\infty(2)}_{ijl} q_l \tag{33}$$

Quite often experimental data are recorded using polarized or unpolarized lasers on powdered samples. If we neglect the surface effects on the Raman tensors, an approximation that is valid for anything but nanocrystals, the Raman spectra are averages over all possible orientation of the crystals and sums over the parallel and perpendicular laser polarizations. The intensities of the two polarized components of the powder spectra, parallel and perpendicular, and the resulting total powder spectra are (Placzek, 1934; Prosandeev *et al*., 2005):

$$\begin{aligned} I_{\parallel}^{powder} &= C(10G_0 + 4G_2) \\ I_{\perp}^{powder} &= C(5G_1 + 3G_2) \\ I_{tot}^{powder} &= I_{\parallel}^{powder} + I_{\perp}^{powder} \end{aligned} \tag{34}$$

where

$$\begin{aligned} G_0 &= \frac{(\alpha_{xx} + \alpha_{yy} + \alpha_z)^2}{3} \\ G_1 &= \frac{(\alpha_{xy} - \alpha_{yz})^2 + (\alpha_{yz} - \alpha_{zx})^2 + (\alpha_{zx} - \alpha_{xy})^2}{2} \\ G_2 &= \frac{(\alpha_{xy} + \alpha_{yz})^2 + (\alpha_{yz} + \alpha_{zx})^2 + (\alpha_{zx} + \alpha_{xy})^2}{2} + \\ &+ \frac{(\alpha_{xx} - \alpha_{yy})^2 + (\alpha_{yy} - \alpha_{zz})^2 + (\alpha_{zz} - \alpha_{xx})^2}{3} \end{aligned} \tag{35}$$

The Raman spectroscopy can sample only the Raman-active modes of a structure. These modes have null wavevector. For centrosymmetric structures, they preserve the symmetry centre; they are labelled *g*, as *gerade*, meaning right (By contrast the infrared-active modes, do not preserve the centre of symmetry and are

thus labelled by *u*, as *ungerade*, not right). Equation 29 gives the Raman tensor of these modes. For non-centrosymmetric structures there are particular modes that can be active in both Raman and infrared, depending on the mode symmetry. In this case the expression for the Raman tensor is modified, as shown in Equation 30. The character tables (Kroumova *et al*., 2003) are employed to determine whether a mode is Raman active, infrared active or silent. Complete lists can be found, for example, on the Bilbao Crystallographic Server.

5. Examples

The first Raman determinations date as early as 1986 (Baroni & Resta, 1986). More recently, as implementations were made available within the large DFT packages, computations of the Raman spectra has shown a powerful predictive power, especially for materials at extreme conditions, and were employed on a large scale.

One target class of materials were the ferroelectrics and piezoelectrics, due to their obvious technological applications. Raman spectra and non-linear optical coefficients have been successfully computed for a series of materials, like multiferroic bismuth ferrite (Hermet *et al*., 2007a), ferroelectric lithium niobate (Hermet *et al*., 2007b or piezoelectric oxynitrides (Caracas & Cohen, 2007).

Calculations of Raman spectra for minerals have received a lot of attention. This approach, due to its predictive power is particularly useful in the study of matter at extreme pressure-temperature conditions. For example, spectra have been already reported for the perovskite and post-perovskite (Caracas & Cohen, 2006), the major minerals of the Earth's lower mantle. It was shown that Raman spectroscopy can be used to identify the phase transition. This is an important aspect as Raman measurements in diamond-anvil cell are usually easier to perform than X-ray crystallography one that requires oftentimes synchrotron radiation.

The same transition can be similarly searched for in analogue materials, like the sesquioxides (Caracas & Cohen, 2007a). Other minerals from the Earth's upper mantle have been studied, too, the theoretical predictions faring pretty well in comparison to experiments. In the case of Mg_2AlO_4 spinel (Caracas & Banigan, 2009), calculations showed that site disorder must be present in order to explain the observed intensity ratios between the major peaks. The symmetrization of the hydrogen bond was studied in aluminium oxy-hydroxide (Tsuchiya *et al*., 2008) and the spectra of Mg_2SiO_4 forsterite were described at ambient conditions (McKeown *et al*., 2010).

Calculations on molecular crystals are efficient, too. The theoretical determination of the Raman spectra of the polymeric phase of nitrogen, stable at pressures beyond megabar, was used to confirm the existence of this phase and to close a long-standing experimental discussion (Eremets *et al*., 2004). The Raman spectra of this phase, the cubic gauche, are dominated by the presence of only one strong peak. The theoretical calculations are in excellent agreement with the *in situ* experimental observations, and came as nice and final confirmation of the existence of this phase (Caracas, 2007). Raman spectroscopy could also be used to identify the transition to the first post-ice-X form of water ice, occurring beyond 4 mbars (Caracas, 2008). In giant ice planets this transition can produce layering towards the basis of their mantles, which influences their convection and thermal state. Finally

computed Raman spectra of the alpha-boron phase confirmed the experimental observation of structural changes occurring around 40 GPa. Based on the complementary analysis an isosymmetrical phase transition has been proposed (Zarechnaya, 2010). But from all these efforts, the Wurm database of computed Raman spectra for minerals (Caracas & Bobocioiu, 2011) remains the largest so far by any comparison.

6. The WURM project

The WURM project consists of building a database with computed physical properties for minerals, from which Raman spectra constitute a central part. Its aims are multiple: providing Raman reference spectra to be used in mineral identification, understanding the mineral Raman spectra, offering a teaching basis for vibrational spectroscopy, reporting theoretical structures, building a repository for a variety of physical properties for minerals.

The computed data are presented on the http://www.wurm.info website, which recently went through a major update. The website is written in php and has a major javascript component that ensures a high level of interactivity with the user. For example the visualization of the crystal structure as well as of the atomic displacement patters of all vibrational modes is realized in Jmol-powered applets incorporated in the website.

The data are distributed through the Common Contents license. In general the philosophy of the WURM project is similar to that of RRUFF (Downs, 2006), hosted at http://rruff.info, in practice offering its theoretical alternative. All the results are exclusively obtained from first-principles calculations performed using DFT and DFPT. We use the local density approximation in the ABINIT implementation (Gonze *et al*., 2002, 2005a, 2009).

For each mineral four classes of data are reported: structural information, parameters of the calculations, dielectric tensors and vibrational information. The structural part contains the unit cell size, the number of atoms and their position. A jmol appl*et al*lows for the visualization of the structure; one unit cell as well as an arbitrary supercell can be equally visualized. The parameters of the calculations contain technical information. The dielectric part reports the dielectric tensors and the Born effective charges. For the moment only the numerical values are given, one of the future developments being oriented towards a visualization of these tensors. For example, the refractive index can be used directly to build a virtual optical microscope. Finally the vibrational part contains (i) one table with the full list of normal modes in the centre of the Brillouin zone and their Raman intensities in absolute or relative values and (ii) one graph with the Raman spectrum for powder. All the cells of the table with the frequencies are clickable – upon click a separate window opens where another jmol applet shows dynamically the atomic displacement pattern corresponding to that particular phonon. The size of the structural representation is again adjustable to any desired supercell dimension. The plot is scalable both horizontally and vertically; representations for powders with parallel or perpendicular laser polarizations as well as for depolarized laser excitation are possible. An example with the spectrum of topaz is shown in Figure 4.

The first minerals to be computed were characterized by relatively simple structures with a limited amount of atoms in the unit cell. More recently, we have addressed more complex structures; we have extensively worked on carbonate minerals, on some sulphate minerals and nesosilicates. We have treated several terms along the plagioclase feldspar solid solution using the alchemical pseudopotential approach (Giantomassi, 2005; Cohen, 2007). While many spectra have their experimental counterpart in RRUFF, a number of spectra are available today only in theory.

The quality of the comparison between calculations and experiments is variable from one structure to the other. In general better agreement is obtained if calculations are performed at the same specific volume as in experiment.

Acknowledgements

The WURM project is sponsored by Michael Scott. Calculations related to the project are performed at the Pole de Simulation et Modelisation Numerique (PSMN) of the Ecole Normale Superieure de Lyon and on the SGI Altix machine JADE of the Centre Informatique National de l'Enseignement Superieur (CINES) through DARI grants stl2816.

References

Altmann, S. L. (1991): Band theory of solids an introduction from the point of view of symmetry. Oxford University Press, Oxford.

Baroni, S., Giannozzi, P. & Testa, A. (1987): Testa, A. Green's-function approach to linear response in solids. *Physical Review Letters* **58**, 1861–1864.

Baroni, S., de Gironcoli, S., Dal Corso, A. & Giannozzi, P. (2001): Phonons and related crystal properties from density-functional perturbation theory. *Reviews Modern Physics* **73**, 515–562.

Baroni, S. & Resta, R. (1986): Ab initio calculation of the low-frequency Raman cross section in silicon, *Physical Review B* **33**, 5969– 5971.

Caracas, R. (2007): Raman spectra and lattice dynamics of cubic gauche nitrogen, *Journal of Chemical Physics* **127**, 144510.

Caracas, R. (2008): Dynamical instabilities of ice X, *Physical Review Letters* **101**, 085502.

Caracas, R., & Banigan, E.J. (2009): Elasticity and Raman spectra of MgAl2O4 spinel from density functional perturbation theory, *Physics Earth Planetary Interiors* **174**, 113-121.

Caracas, R., & Bobocioiu, E. (2011): The WURM project - a freely available web-based repository of computed physical data for minerals, *American Mineralogist* **96**, 437-444.

Caracas, R. & Cohen, R.E. (2006): Theoretical determination of the Raman spectra of $MgSiO_3$ perovskite and post-perovskite at high pressure, *Geophysical Research Letters* **33**, No. 12, L12S05.

Caracas, R., & Cohen R.E. (2007): Prediction of polar ordered oxynitrides, *Applied Physics Letters* **91**, 092902.

Caracas, R. & Cohen, R.E. (2007a): Post-perovskite phase in selected sesquioxides from density-functional calculations, *Physical Review B*, **76**, 184101.

Caracas, R. & Gonze, X. (2005): First-principles study of materials involved in incommensurate transitions. *Zeitschrift fuer Kristallografie*, **220**, 511–520.

Caracas, R. & Gonze, X. (2010): Lattice Dynamics and Thermodynamical Properties, In: Thermodynamic Properties of Solids: Experiment and Modeling, Edited by S. L. Chaplot, R. Mittal, and N. Choudhury, WILEY-VCH Verlag, Weinheim

Cardona, M. (1982): Light Scattering in Solids II: Basic Concepts and Instrumentation, vol. **50**, Topics in Applied Physics, edited by M. Cardona and G. Güntherodt, pp. 19– 168, Springer, New York.

Cohen, M.L. (2007): Quantum alchemy. In: Keinan, E., Schechter, I. (Eds.), Chemistry for the 21st century. Wiley-VCH.

Downs, R.T. (2006): The RRUFF Project: an integrated study of the chemistry, crystallography, Raman and infrared spectroscopy of minerals. Program and Abstracts of the 19th General Meeting of the International Mineralogical Association in Kobe, Japan. O03-13.

Eremets, M., Gavriliuk,. A.G., Trojan, I.A., Dzvienko, D.A. & Boehler, R., (2004): Single-bonded cubic form of nitrogen, *Nature Materials* **3**, 558.

Giantomassi, M., Boeri, L., Bachelet, G.B. (2005): Electrons and phonons in the ternary alloy CaAl2−xSix as a function of composition. *Physical Review B* **72**, 224512.

Gironcoli, S., de (1995): Lattice dynamics of metals from density-functional perturbation theory. *Physical Review B* **51**, 6773–6778.

Gonze, X. (1995): Adiabatic density functional perturbation theory. *Physical Review A* **52**, 1096–1114.

Gonze, X. (1997): First-principle responses of solids to atomic displacements and homogeneous electric fields implementation of a conjugate-gradient algorithm. *Physical Review B* **55**, 10337–10354.

Gonze, X., Allan, D. C. & Teter, M. P. (1992): M. P. Dielectric tensor, effective charges and phonon in α-quartz by variational density-functional perturbation theory. *Physical Review Letters* **68**, 3603–3606.

Gonze, X., Amadon, B., Anglade, P.-M., Beuken, J.-M., Bottin, F., Boulanger, P., Bruneval, F., Caliste, D., Caracas, R., M. Côté, Deutsch, T., Genovesi, L., Ghosez, Ph., Giantomassi, M., Goedecker, S., Hamann, D.R., Hermet, P., Jollet, F., Jomard, G., Leroux, S., Mancini, M., Mazevet, S., Oliveira, M.J.T., On-ida, G., Pouillon, Y., Rangel, T., Rignanese, G.-M., Sangalli, D., Shaltaf, R., Tor-rent, M., Verstraete, M.J., Zerah G., and Zwanziger, J.W. (2009): ABINIT: First-principles approach to material and nanosystem properties, *Computer Physics Communications* **180**, 2582-2615.

Gonze, X., Beuken, J.-M., Caracas, R., Detraux, F., Fuchs, M., Rignanese, G.-M., Sindic, L., Verstraete, M., Zerah, G., Jollet, F., Torrent, M., Roy, A., Mikami, M., Ghosez, Ph., Raty, J.-Y. & Allan, D. C. (2002): First-principle computation of material properties the ABINIT software project. *Computational Materials Science* **25**, 478–492. [http//www.abinit.org]

Gonze, X. & Lee C. (1997): Dynamical matrices, Born effective charges, dielectric permittivity tensors, and interatomic force constants from density-functional perturbation theory. *Physical Review B* **55**, 10355–10368.

Gonze, X. Rignanese, G.-M., & Caracas, R. (2005): First-principle studies of the lattice dynamics of crystals, and related properties, *Zeitschrift fuer Kristallografie*, **220**, 458-472.

Gonze, X., Rignanese, G.-M., Verstraete, M., Beuken, J.-M., Pouillon, Y., Caracas, R., Jollet, F., Torrent, M., Zerah, G., Mikami, M., Ghosez, Ph., Veithen, M., Raty, J.-Y., Olevano, V., Bruneval, F., Reining, L., Godby, R., Onida, G., Hamann, D. R. & Allan, D. C. (2005a): A brief introduction to the ABINIT software package. *Zeitschrift fuer Kristallografie*, **220**, 558–562.

Gonze, X. & Vigneron, J.-P. (1989): Density-functional approach to nonlinear-response coefficients of solids. *Physical Review B* **49**, 13120–13128.

Hayes, W., & Loudon, R., (1978) Scattering of Light by Crystals. John Wiley, Hoboken, New Jersey, 113 pp.

Hermet, P., Goffinet, M., Kreisel, J. & Ghosez, Ph. (2007a): Raman and infrared spectra of multiferroic bismuth ferrite from first-principles, *Physical Review B* **75**, 220102(R).

Hermet, P., Veithen, M. & Ghosez, Ph., (2007b): First-principles calculations of the nonlinear optical susceptibilities and Raman scattering spectra of lithium niobate, *Journal of Physics: Condensed Matter* **19**, 456202.

Hohenberg, P. & Kohn, W. (1964): Inhomogeneous electron gas. *Physical Review* **136**, B864-B871.

Kohn, W., & Sham, L. J. (1965): Self-consistent equations including exchange and correlation effects. *Physical Review* **140**, A1133–A1138.

Kroumova, E. , Aroyo, M.I., Perez Mato, J.M., Kirov, A., Capillas, C., Ivantchev, S., & Wondratschek, H. (2003): Bilbao Crystallographic Server: useful databases and tools for phase transitions studies. *Phase Transitions* **76**, 155-170.

Landau, L. & Lifschits, E. (1960): Electrodynamics of Continuous Media. Pergamon Press.

Lazzeri, M. & Mauri, F. (2003): First-principles calculation of vibrational raman spectra in large systems: Signature of small rings in crystalline SiO_2, *Physical Review Letters*, 90, 36– 401.

Maradudin, A. A., Montroll, E. W., Weiss, G. H. & Ipatova, I. P. (1971): Theory of lattice dynamics in the harmonic approximation in Solid State Physics (Eds. H. E. Ehrenreich; F. Seitz; D. Turnbull). Academic Press, New York.

Martin, R.M. (2004): Electronic Structure: Basic Theory and Practical Methods, Cambridge University Press.

McKeown, D.A., Bell, M.I., & Caracas, R. (2010): Theoretical determination of the Raman spectra of single-crystal forsterite (Mg_2SiO_4). *American Mineralogist*, 95, 980-986.

Monkhorst, H.J., Pack, J.D. (1976): Special points for Brillouin-zone integrations. *Physical Review B* **13**, 5188–5192.

Nunes, R.W., & Gonze, X. (2001): Berry-phase treatment of the homogeneous electric field perturbation in insulators, *Physical Review B* **63**, 155107.

Pawley, G.S. (1974): Phonon symmetries determined from space-group diagrams, *Acta Crystallographica* **A30**, 585-596

Payne, M.C., Teter, M.P., Allan, D.C, Arias, T.A., & Joannopoulos, J. D. (1992): Iterative minimization techniques for ab initio total-energy calculations: molecular dynamics and conjugate gradients, *Reviews in Modern Physics* **64**, 1045.

Perez-Mato, J.M., Aroyo, M., Hlinka, J., Quilichini, M., & Currat, R. (1998) Phonon Symmetry Selection Rules for Inelastic Neutron Scattering, *Physical Review Letters* **81**, 2462–2465.

Placzek, G. (1934): Rayleigh-Streuung und Raman-Effekt, in Handbuch der Radiologie, vol. 6, edited by G. Marx, pp. 205–374, Akademische, Frankfurt-Main, Germany.

Prosandeev, S. A., Waghmare, U., Levin, I. & Maslar, J. (2005): First-order Raman spectra of AB0 1/2B00 1/2O3 double perovskites, *Physical Review B* **71**, 214–307.

Putrino, A., Sebastiani, D. & Parrinello, M. (2000): Generalized variational density functional perturbation theory. *Journal of Chemical Physics* 113, 7102–7109.

Reynard, B., & Caracas, R. (2009): H/D isotopic fractionation of brucite Mg(OH)2 with water from vibrational spectroscopy and ab initio modelling, *Chemical Geology* **262**, 159-168.

Rull, F., et al. (2012) Theory of Raman Spectroscopy. Pp. X–Y. in: *Applications of Raman Spectroscopy to Earth Sciences and Cultural Heritage* (J. Dubessy & F. Rull, editors). EMU Note Book.

Srivastava, G.P. (1990): *The physics of phonons*. Taylor and Francis, 438 pps.

Tsuchiya, J., Tsuchiya T. & R.M. Wentzcovitch (2008): Vibrational properties of δ-AlOOH under pressure, *American Mineralogist* **93**, 477-482.

Veithen, M., Gonze, X., & Ghosez, Ph. (2005): Non-linear optical susceptibilities, Raman efficiencies and electro-optic tensors from first-principles density functional perturbation theory. *Physical Review B* **71**, 125107.

Zarechnaya, E., Dubrovinskaia, N., Caracas, R., Merlini, M., Hanfland, M., Filinchuk, Y., Chernyshov, D., Dmitriev, V., & Dubrovinsky, L. (2010): Pressure-Induced Isostructural Phase Transformation in γ-B28, *Physical Review B* **82**, 184111.

Figures.

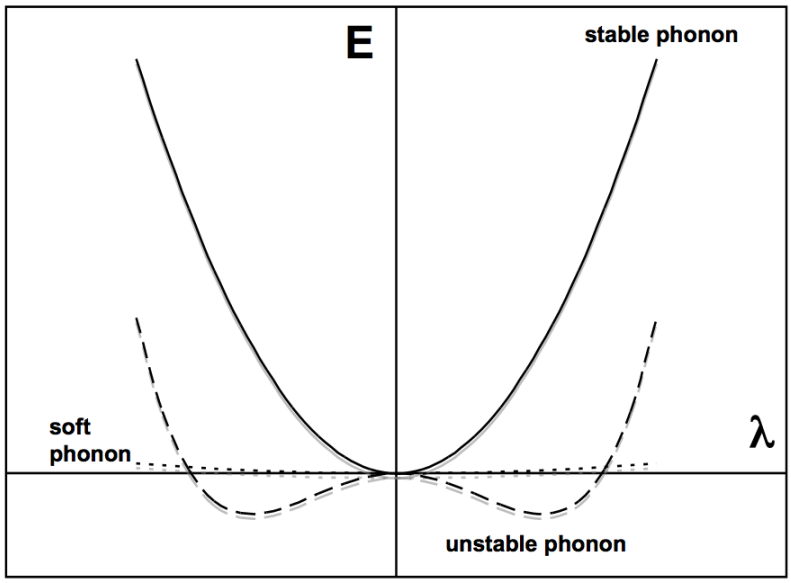

Figure 1. Schematic representation of the energy variation as a function of the atomic displacement (λ), as perturbation from the equilibrium position. Continuous line: single-well potential line; dashed line: ; dotted line: soft phonon potential

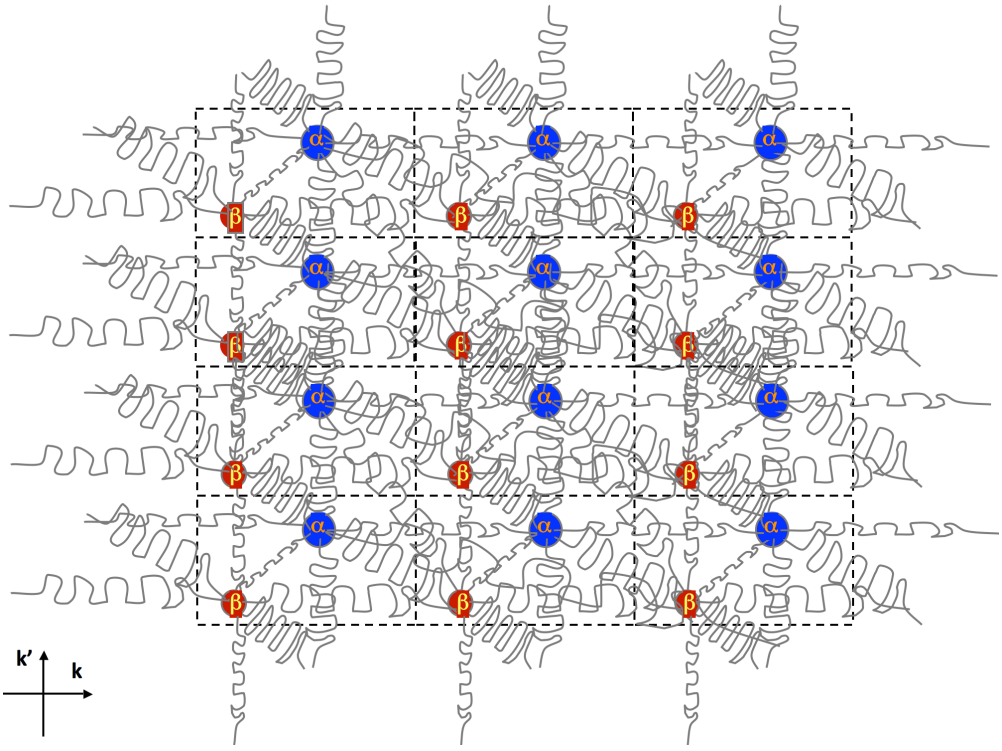

Figure 2. The crystal structure is seen as an elastic lattice in the quasiharmonic approximation. The interatomic force constants correspond to the constants of the elastic resort tying the atoms together.

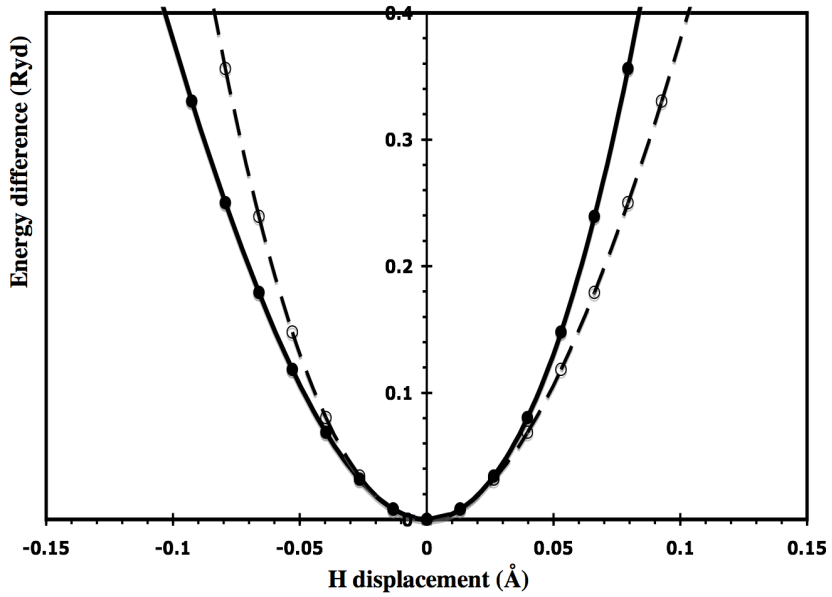

Figure 3. The exact calculation of the energy vs. atomic perturbation yields a non-symmetrical curve, because of the non-equivalence between the attraction and repulsion components of the interatomic force constants. In the quasiharmonic approximation this curve is taken symmetrical (continuous curve with filled circle symbols). The two dashed lines show the effect of symmetrization, which changes the curvature at zero and thus eventually affects the phonon frequency.

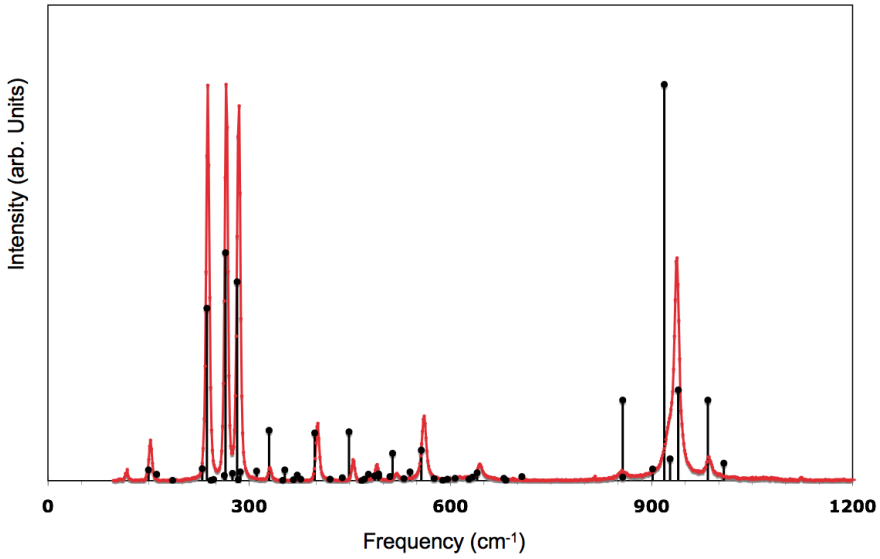

Figure 4. Comparison between computed in WURM (vertical bars) and measured in RRUFF (continuous line) Raman spectra of topaz, $Al_2SiO_4F_2$. The agreement between WURM and RRUFF is very good. Slight peak shifts and differences in intensity recorded at high frequency are mostly due to the presence of OH in experiment, while calculations are for water-free composition.